

Simulation and Control of a Tether-Actuated Closing Mechanism for Net-Based Capture of Space Debris



Corey Miles

Supervised by Prof. Inna Sharf
Co-Supervised by Eleonora Botta
Department of Mechanical Engineering
McGill University

A thesis submitted to McGill University in partial fulfilment of the requirements of the Undergraduate Honours Program.

December 2018

Acknowledgements

I am deeply grateful to Professor Inna Sharf for her guidance throughout the process of my honours thesis. She gave me the freedom to direct this research, and motivated me to improve my research skills along the way. In the last few weeks, she gave me the support I needed to overcome several challenges and I appreciate the time she devoted to answering my many questions and concerns. I finish my honours thesis feeling inspired to pursue research on a similar topic at the graduate level.

Much of this work would not have been possible without the help and support of Eleonora Botta. I am thankful to her for helping me through many hours of debugging the simulator, and for passing it on to me in the first place. I am also thankful for her responsiveness and desire to help, despite working full time outside of McGill.

Abstract

The growth of space debris in Earth's orbit is recognized as a serious threat to future space missions. To contain the growth of space debris, active removal of large objects such as defunct satellites and spent rocket upper stages is needed. A promising solution to this problem uses tethered-nets. A net is released from a chaser spacecraft toward a target debris; the net entangles the debris and the tether provides a flexible link between chaser and debris to tug the debris to a disposal orbit. A net-closing mechanism is needed to contain the debris. This work is focused on the simulation and control of a tether-actuated closing mechanism. In this concept, the tether is looped through the center of the net and around the perimeter, and spooling the tether in, by means of a winch, draws the net perimeter closed. A model of the tethered-net active debris removal system with the tether-actuated closing mechanism is developed. Through simulations, the deployment of the tethered-net is evaluated and the characteristics of deployment are used to determine a nominal capture scenario. Open loop and closed loop control strategies are employed for the capture and containment of a desired target debris. The tether-actuated closing mechanism shows promise, in that containment of debris is possible with simple winching controls applied to the tether.

Résumé

La croissance des débris spatiaux en orbite terrestre est reconnue comme une grave menace pour les futures missions spatiales. Pour contenir la croissance des débris spatiaux, il est nécessaire d'enlever activement les objets de grande taille tels que les satellites défunts et les étages supérieurs des fusées. Une solution potentielle à ce problème utilise des filets attachés. Un filet est libéré d'un vaisseau spatial ("chasseur") vers le débris ciblé; le filet emmêle les débris et l'attache offre un lien flexible entre le chasseur et le débris pour ramener le débris vers une orbite de destruction. Un mécanisme de fermeture du filet est nécessaire pour contenir le débris. Ce travail est axé sur la simulation et le contrôle d'un mécanisme de fermeture actionné par une attache. Dans ce concept, l'attache est bouclée au centre du filet et autour du périmètre, puis l'enroulement au moyen d'un treuil va tirer le périmètre du filet et le fermer. Un modèle est développé d'un système d'élimination active des débris à l'aide d'un filet attaché avec un mécanisme de fermeture actionné par une attache. Au moyen de simulations, le déploiement du filet attaché est évalué et les caractéristiques de déploiement sont utilisées pour déterminer un scénario de capture nominal. Des stratégies de contrôle en boucle ouverte et en boucle fermée sont utilisées pour la capture et le confinement des débris cibles souhaités. Le mécanisme de fermeture actionné par l'attache a beaucoup de potentiel, dans la mesure où le confinement des débris est possible avec de simples contrôles de treillage appliqués à l'attache.

Table of contents

List of figures	ix
List of tables	xi
1 Introduction	1
1.1 Background	1
1.2 Motivation	3
1.3 Thesis Objectives	5
2 Modelling the System in Vortex Dynamics	7
2.1 Net and Tether Representation	7
2.1.1 Standard Lumped Parameter Model of the Net	7
2.1.2 Flexible Cable Model of the Tether	9
2.2 The Tether Actuated Closing Mechanism	10
2.2.1 Single Tether Configuration	12
2.2.2 Double Tether Configuration	12
2.2.3 Model of the Winch	12
2.3 System Assembly	15
3 Simulation and Analysis of Deployment	17
3.1 Initial Conditions	17
3.2 Deployment Quality Indices	18
3.3 Simulation Parameters	19
3.4 Deployment with a Free Tether	20
4 Control of the Tether-Actuated Closing Mechanism	25
4.1 Capture Dynamics	25
4.1.1 Target Debris	26
4.1.2 Criteria for Capture and Containment of Debris	27
4.1.3 Nominal Capture Scenario	27

4.2	Open Loop Control Strategy	28
4.2.1	Measurable Parameters	29
4.2.2	Angular Velocity Control of the Winch	30
4.3	Closed Loop Control Strategy	33
4.3.1	PD Tension Control	33
4.3.2	Gain Scheduling	34
4.4	Discussion of Results	37
5	Conclusion	41
5.1	Main Findings	41
5.2	Suggestions for Future Work	42
	References	45

List of figures

1.1	Population of objects in Earth's orbit	2
1.2	ESA's e.Deorbit system	4
1.3	Tethered-net ADR concept	4
2.1	Standard lumped parameter model of the net	9
2.2	Flexible cable model of the tether	10
2.3	Tether-actuated closing mechanism with four tethers.	11
2.4	Single and double-tether actuated closing mechanism designs	13
2.5	Reel mechanism conceptual design	13
2.6	Model of the winch	14
2.7	Assembly of the system.	15
3.1	Snapshots of deployment	22
3.2	Net and tether deployment characteristics.	23
3.3	Tension in the perimeter segments of the tether.	24
4.1	Model of a Zenit 2 upper stage in Vortex Dynamics.	26
4.2	Nominal capture scenario.	29
4.3	Collision between net and debris with the tether-actuated closing mechanism free to spool out.	32
4.4	Open loop angular velocity control of the winch.	32
4.5	PD tension control of the tether-actuated closing mechanism.	34
4.6	Results from simulation of debris capture with PD tension control with gain scheduling	35
4.7	Snap shots from simulation of debris capture with PD tension control and gain scheduling.	37
4.8	PD tension control with gain scheduling and emulated thruster control of the chaser spacecraft.	38

List of tables

- 3.1 System properties 20
- 3.2 Initial conditions 21

- 4.1 Initial conditions for simulation of capture. 28
- 4.2 Reference tension and control gains 33

Chapter 1

Introduction

1.1 Background

Since the launch of Sputnik 1 in 1957, satellites have become an integral part of society and continue to be at the forefront of many industries including space exploration, communication technologies, and environmental monitoring. Unfortunately, the amount of space debris in Earth's orbit has increased drastically due to the growing use of satellites, and resulting collisions between active and inactive objects. The Kessler Syndrome, proposed by Donald J. Kessler in 1978, is a scenario in which the density of objects in Earth's orbit is high enough that each collision between objects generates more debris and increases the likelihood of further collisions, causing the amount of debris in orbit to grow exponentially [1]. This is potentially catastrophic, as it would render much of Earth's orbit unusable for several generations. Organizations such as NASA and ESA have been tracking both active and inactive objects in Earth's orbit for the past few decades. As of November 7 2018, the US Space Surveillance Network is tracking over 19000 objects greater than 10 cm in diameter in Earth's orbit. Other than just over 2000 active payloads, this population is dominated by debris including fragments from collisions, spent rocket upper stages, and retired payloads [2]. A model of the population of active and inactive objects in orbit as of January 2017 is shown in Fig 1.1.

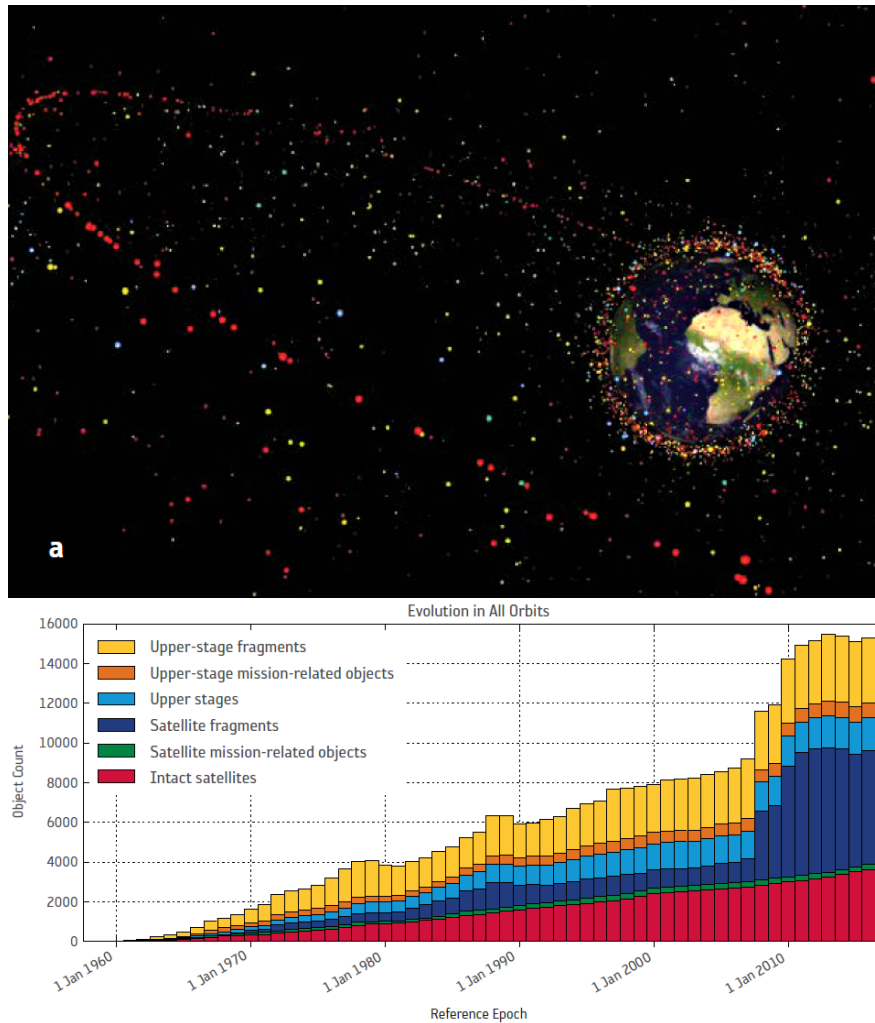


Fig. 1.1 Model of the debris population of objects larger than 1 m as of January 2017 [3].

The debris population in Low Earth Orbit (LEO) poses the greatest threat, as it has reached a point where the population of debris would still increase due to the cascade effect of collisions even if all future missions were suspended [4]. This premise is supported by a major collision in 2007 during an attempted anti-satellite test by the Chinese Space Program, and an accidental collision between two satellites, Iridium-33 and Cosmos-2251, in 2009. These collisions alone caused increases in the debris population of 34% and 17% respectively [3]. As more and more satellites and other payloads are launched into LEO each year, the likelihood of additional major collision events will only increase. It is evident that the Kessler Syndrome could soon become a reality, and thus the need

for systems to mitigate space debris is essential for keeping the window of operation open for future space missions.

1.2 Motivation

Many researchers have been developing Active Debris Removal (ADR) systems in an effort to slow down the growth of debris in LEO. The general requirement for ADR states that 5-10 high risk objects must be de-orbited each year from the most crowded regions in order to prevent the debris population from becoming uncontrollable [2]. Wiedemann proposed a sorting of debris which consists of 24 high risk objects with the highest probabilities of catastrophic collisions. The list includes Envisat, a European satellite that went silent in 2012, and over 20 Zenit rocket upper stages [5]. These objects are known to be orbiting at inclinations between 82.5° and 83.5° and at altitudes close to 1000km [6]. A typical ADR system consists of a chaser spacecraft and several de-orbiting devices, each with a unique design and functionality. Over the past few years, ESA has been involved in the design and planning phase of their eDeorbit mission with the goal of capturing Envisat by 2024, and they have been working with several research institutions and companies to develop the systems that will be used for the mission, which consists of either a robotic arm or a tethered-net. Fig 1.2 shows their proposed robotic arm capturing mechanism. Upon rendezvous with Envisat, the arm extends from a small chaser spacecraft and is equipped with a gripper to clamp onto the Launch Adapter Ring (LAR) of the satellite. Once the gripper has closed, an additional clamping mechanism secures the chaser to the side of Envisat so that the combined system can now be controlled by the spacecraft's thrusters [7]. A major disadvantage of this capturing method is that a complicated rendezvous phase is needed. Also, accurate relative position and velocity between target and chaser is essential. In addition, the rigid connection between target and spacecraft raises

the possibility of the two systems colliding with each other if the capture mechanism fails, possibly creating more debris if the impact is violent.

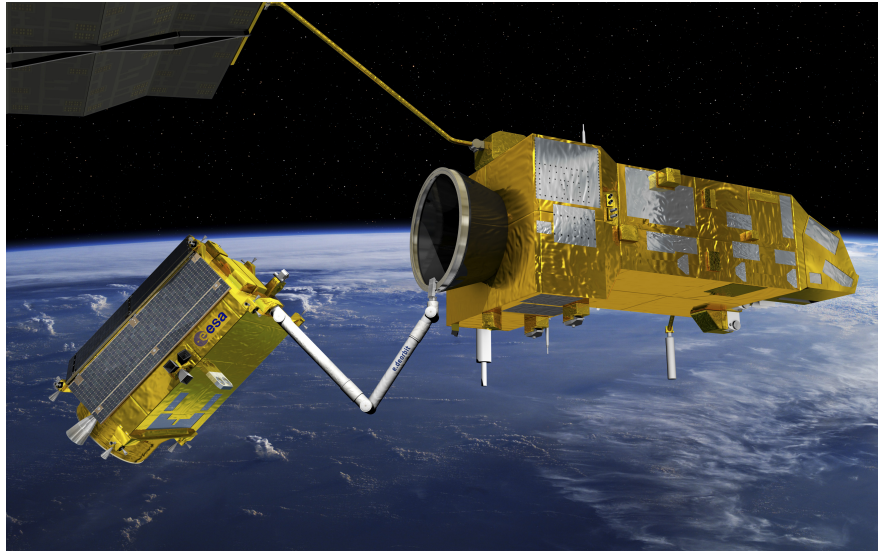


Fig. 1.2 Illustration of ESA's robotic arm capturing system gripping the LAR of Envisat [7].

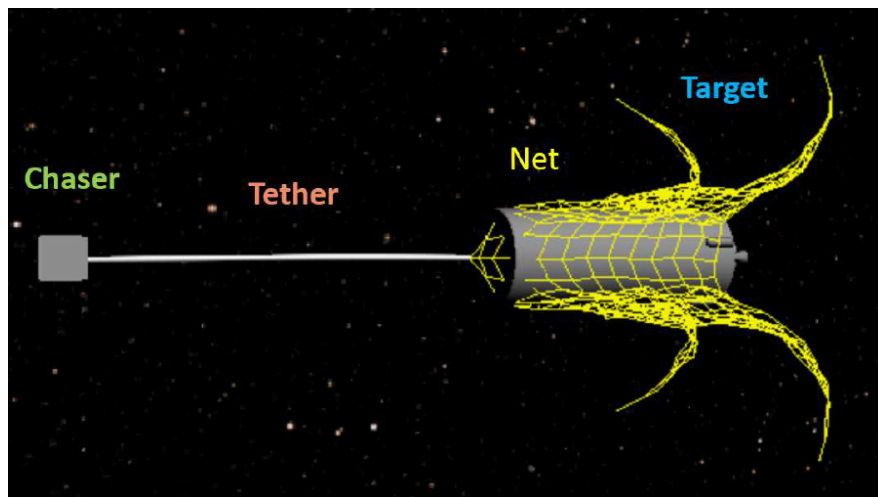


Fig. 1.3 Illustration of the tethered-net ADR concept [8]

A promising alternative debris capturing method that would eliminate some of the risks mentioned above uses flexible tethered-nets. A typical tethered-net ADR system is shown in Fig 1.3 and it has several advantages: it allows a large distance between chaser spacecraft and debris such that close rendezvous and docking with the debris is not required; the size and shape of the debris are not

critical to the success of the mission; and lastly, it is flexible, lightweight, easy to manufacture, and therefore cost effective.

The net is released from a *chaser spacecraft* by ejecting four corner masses outward in the direction of the target debris. The corner masses deploy the net and aid in "wrapping" the net around the debris. Recent research by Botta et al. has shown that a net closing mechanism is needed to ensure that the net remains "wrapped" around the debris when tension is applied to the tether, otherwise the net will slip-off [8]. One such closing mechanism proposed by Sharf et al. [9] is a *tether-actuated closing mechanism*, in which the main tether extends from the chaser spacecraft and is looped through the center of the net and around the perimeter. Tightening the tether by means of a reeling mechanism, such as a winch, would reduce the perimeter of the net thereby containing the debris [9]. Experiments with a tether-actuated closing mechanism were carried out by Thomsen in 2017 and compared to results from simulations of deployment of tethered-nets [9]. The overarching goal of this thesis is to gain further insight into the feasibility of net-based capture of space debris with a tether-actuated closing mechanism.

1.3 Thesis Objectives

Much of this work extends on the research of Eleonora Botta (2017) [8] who designed a simulator for capture of space debris with tethered-nets. Botta demonstrated that a tether-actuated closing mechanism could be used to secure debris in the net after capture, but limitations in the modelling and control of the closing mechanism were reported. Using Vortex Dynamics, a multibody dynamics simulation tool by local company CM Labs, this thesis aims at overcoming the limitations of the previous work and at gaining additional insight on tether-actuated closing mechanisms. The research

objectives of this thesis are split into three parts, with each one building upon the last.

The first goal is to develop a model of the tethered-net ADR system with the tether-actuated closing mechanism using the Vortex Dynamics simulator. The modelling of the net and tether is drawn directly from the work of Botta, while two improved design configurations of the tether-actuated closing mechanism are implemented. Existing research on the design of reeling mechanisms for tethered-nets is used in describing the model of the winch employed in the simulator.

Following this, simulation and analysis of deployment of the tethered-net system is performed. The effect of the tether-actuated closing mechanism on key deployment quality indices drawn from literature is discussed. The characteristics of the net and tether during deployment are then used to determine a nominal capture scenario.

Finally, open loop and closed loop control of the tether-actuated closing mechanism is employed in an attempt to capture and contain a desired target debris. The design of the control strategies depends on the measurable parameters and performance limits that would be present in a real tethered-net ADR system.

Chapter 2

Modelling the System in Vortex Dynamics

This chapter deals with the modelling in Vortex Dynamics of the net, tether, and tether actuated closing mechanism, as well as the assembly of the system with the chaser spacecraft. It is important to have a strong understanding of the dynamics model of the system to better understand the simulations of deployment and capture presented in Chapter 3 and Chapter 4.

2.1 Net and Tether Representation

2.1.1 Standard Lumped Parameter Model of the Net

A lumped parameter model for simulating of the dynamics of flexible space-nets is widely agreed upon in the literature. The model employed for this research is based on previous work by Botta on the dynamics of tether-net systems for ADR [8]. The net takes a square geometry with four corner masses attached to the corners of the net via corner threads. The total mass of the net is lumped into a finite number of spherical rigid bodies, called nodes, located at the physical knots of the net. If there are N nodes along the side of the net along with four corner masses, the total number of nodes is $N^2 + 4$ and the total number of threads is $2N(N - 1) + 4$. We define the *net proper* as the set of the first N^2 nodes and $2N(N - 1)$ threads, excluding the corner masses and corner threads. Fig 2.1

shows a visualization of the lumped parameter model of the net in Vortex Dynamics. The inertial properties of the nodes are determined by the geometric and physical properties of the net and corner masses: the radius of the net threads r_{net} and of the corner threads r_{CT} , and the density of the net material ρ_{Net} and of the corner mass material ρ_{CM} , and lastly the length of the net threads l_{net} and of the corner threads l_{CT} . The corner masses each have a mass m_{CM} . The mass lumped onto the i -th node of the net is the sum of half the mass of each of the threads adjacent to the i -th node. The mass of the net proper is the sum of the mass of all N^2 nodes and is denoted M_{net} . The total mass is then the mass of the net proper plus the mass of the four corner masses: $M_{total} = M_{net} + M_{CM}$, where M_{CM} is the sum of the mass of all four corner masses.

Axial stiffness properties of the net threads are represented by massless springs between the nodes, and energy dissipation is accounted for by adding dampers in parallel to these springs. The unstretched length of the net threads is equal to the mesh length of the net, l_{mesh} and for the corner threads it is l_{CT} . The threads can only experience positive tension force; any compression of the threads causes them to go slack. The tension in the k -th thread is given by:

$$\mathbf{T}_k = \begin{cases} T_k \mathbf{e}_k & \text{for } l_k > l_{mesh} \\ \mathbf{0} & \text{for } l_k < l_{mesh} \end{cases} \quad (2.1)$$

The spring stiffness of the threads depends on the Young's modulus E_{net} of the net material, the thread radius and the mesh length. The amount of damping depends on the net's natural frequency, the stiffness, and the damping coefficient of the net material. Important to note is that the standard lumped parameter model considers only stiffness and damping along the axis of each thread denoted

as \mathbf{e}_k in Equation 2.1, and as a result bending stiffness in the net is not accounted for. Lumped parameter models augmented with bending stiffness have been studied [8], but the standard model was chosen for this work.

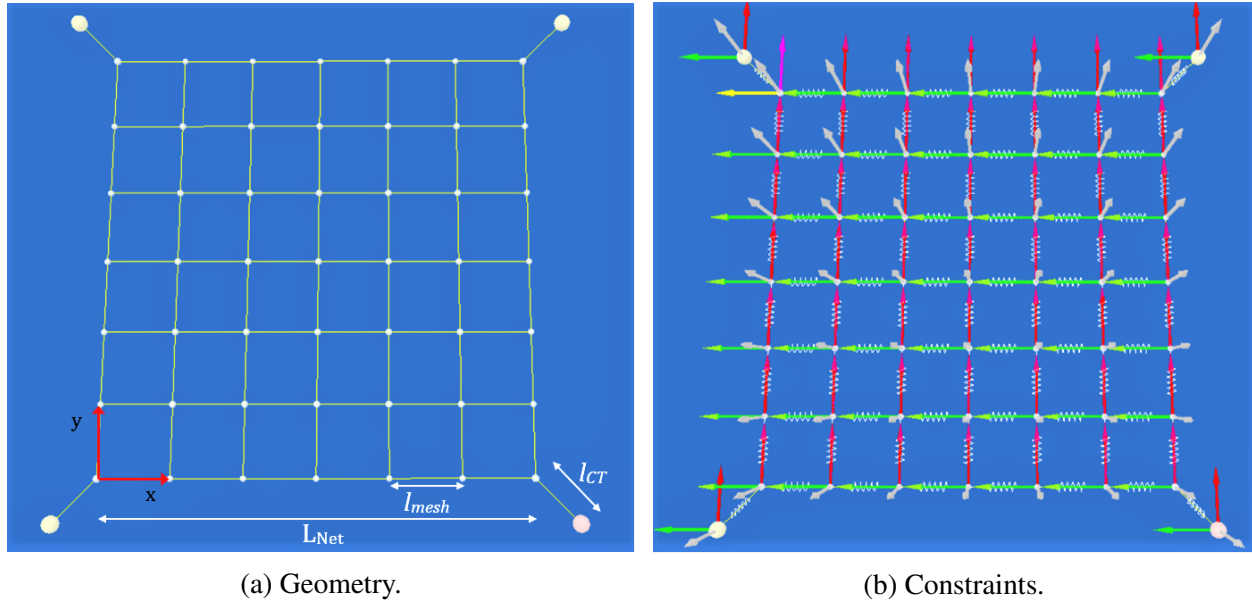


Fig. 2.1 Visualization of the standard lumped parameter model of the net in Vortex Dynamics.

2.1.2 Flexible Cable Model of the Tether

Vortex Dynamic's has its own model for flexible cable systems. The tether is passed through a series of points: a winch; a pulley; a ring; or an attachment point. The portion of the tether between two points is called a *segment*. A segment is discretized into a series of slender rigid bodies with a prescribed collision geometry. Each segment can have a flexible or non-flexible definition. The rigid bodies, called *sections*, are connected by cylindrical joints that, when the segment has a flexible definition, hold elastic bending, torsion and elongation characteristics which are determined by the properties of the tether material; the density ρ_t , the Young's modulus E_t , the tether's radius r_t , and the damping ratio. An illustration of the cylindrical constraints in the flexible cable model is shown in Fig 2.2.

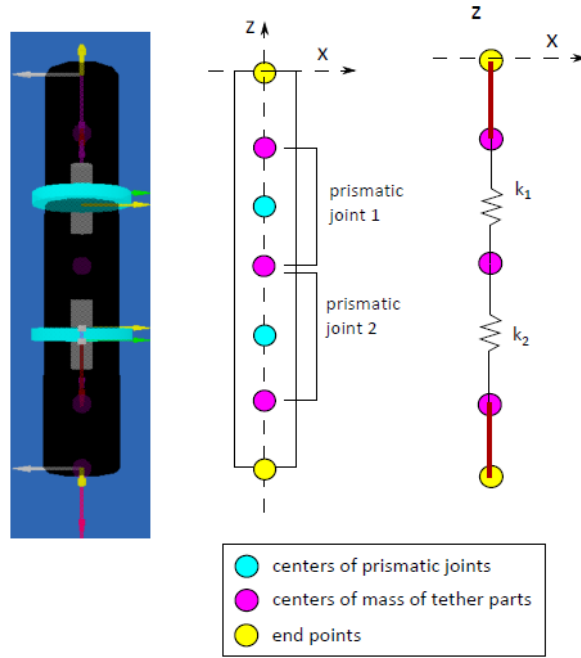


Fig. 2.2 Visualization of a flexible cable in Vortex dynamics [8].

For a cable segment with n_s sections there will be $n_s - 1$ cylindrical joints and thus the effective flexible length of each tether segment is the total length of the segment multiplied by $(n_s - 1)/n_s$. Botta performed several benchmark tests to verify the flexible cable model of the tether, and it was observed that the physical axial and bending stiffness of the tether are given by:

$$k_{a,eff} = EA(n_s - 1)/n_s \quad (2.2)$$

$$k_{b,eff} = EI(n_s - 1)/n_s$$

where E is the Young's modulus of the tether material, A is the tether's cross sectional area and I is the area moment of inertia of the tether's cross section [8].

2.2 The Tether Actuated Closing Mechanism

The tether actuated closing mechanism proposed by Sharf et al. in [9] is modelled by looping the tether through a series of frictionless, massless rings, which are attached to the central node of the net and to several nodes around the perimeter. These rings constrain the tether to the corresponding

nodes of the net, while allowing the tether to slide through them along a specified axis as the length of the tether changes. The end of the tether is secured to a final attachment point at one of the corners of the net proper such that the perimeter of the net is fully enclosed by the tether. Reeling the tether in would shorten the tether length and thus pull the net perimeter closed. Therefore, the first segment of the tether is attached to a reeling mechanism. Increasing the number of tethers in the mechanism can increase the rate at which the net perimeter closes with the same winching rate. The total length of the tether is L_t . If the tether is reeled in by a winch at a constant rate \dot{L}_t and n_t is the number of tethers used for the mechanism, then the rate at which the perimeter length decreases is $n_t \dot{L}_t$. A 4-tether-actuated closing mechanism implemented by Botta is shown in Fig 2.3. However, having 4 separate tethers is impractical and increases the complexity of the system. In this thesis, two simpler configurations for the closing mechanism are implemented and are described in the rest of this section.

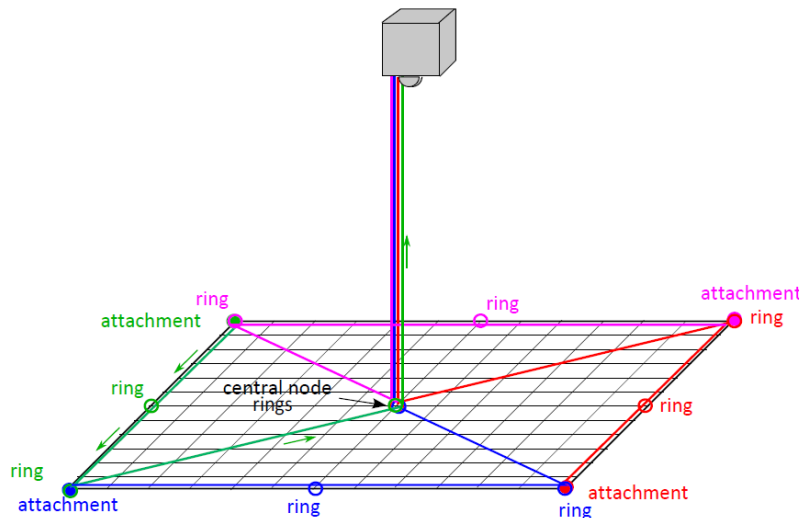


Fig. 2.3 Tether-actuated closing mechanism with four tethers.

2.2.1 Single Tether Configuration

A single-tether actuated closing mechanism with 1 ring at the center of the net and 16 equally spaced perimeter rings is shown in Fig 2.4 (a) and is the simplest design of the proposed closing mechanism. However, this configuration has some limitations. For a single tether a high winching rate would be needed to achieve a desired rate of closure, and the asymmetric design could lead to poor deployment. In fact, this configuration results in very poor deployment, as will be demonstrated in Chapter 3.

2.2.2 Double Tether Configuration

A double tether-actuated closing mechanism can eliminate these problems and is shown in Fig 2.4 (b). Each tether passes through a ring at the central node of the net and around one half of the perimeter in opposite directions, with final attachment points at opposite corners of the net proper. This improves the symmetry of the tether-net system. In addition, the rate of change of the portion of the tether around the perimeter of the net is now twice as fast as the single tether-actuated closing mechanism with the same winching rate.

2.2.3 Model of the Winch

Several reel mechanisms for deployment and retrieval of tethered space systems have been designed and implemented, including the Propulsive Small Expendable-tether Deployer System (ProSEDS) developed at NASA's Marshall Space Flight Center [10]. This system demonstrated the use of a tether to de-orbit a small payload. ESA has also done experiments with space-tethers, such as the YES2 satellite which aimed to demonstrate a tether-assisted re-entry of a payload into Earth's atmosphere [11]. Each of these systems included some form of reeling mechanism for deploying

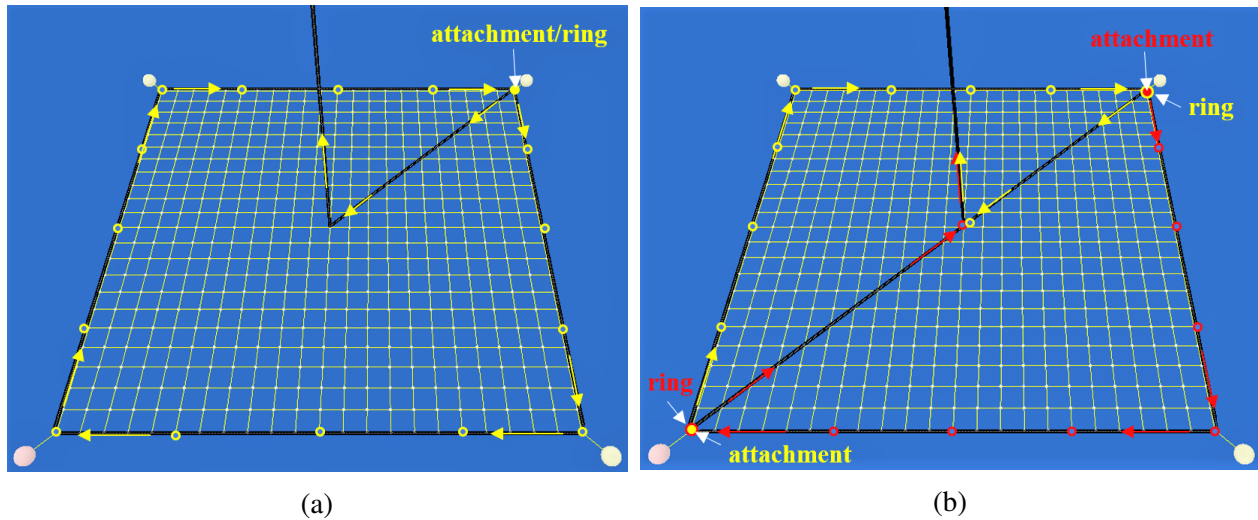


Fig. 2.4 (a) Single tether closing mechanism: Yellow arrows indicate the direction in which tether length changes as it is spooled in. (b) Double tether closing mechanism: The tethers split at the center ring and are looped around the net in opposite directions. The attachment for the red tether and the corner ring for the yellow tether share the same corner node of the net, and vice versa at the opposite corner.

the tether. Recently, research has been carried out on how to control the tether in an ADR situation. Figure 2.5 shows a conceptual design of a reel mechanism by Lanzani (2014) which consists of a main reel, a level wind, guide surfaces, a grip pulley for tensioning the tether, and a tension sensor [12]. The main reel is powered by an electric motor and also incorporates an electrodynamic brake when a constant tether length is desired.

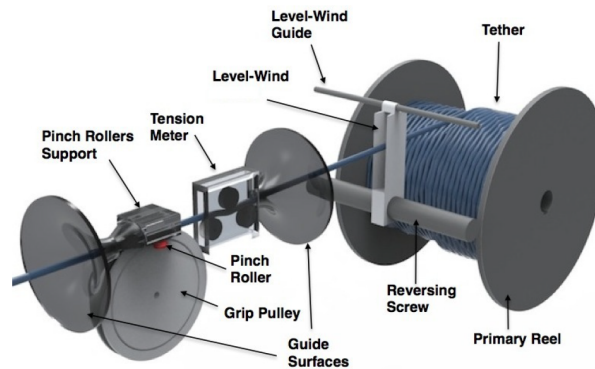


Fig. 2.5 Conceptual design of a reel mechanism developed by Lanzani

For the purpose of this thesis the reeling mechanism is simplified to a winch, modelled as a cylindrical rigid body with length l_w , radius r_w and mass m_w , and coupled directly to a motor represented by a *hinge* constraint in Vortex Dynamics. This constraint allows the tether to be free to spool out, locked, or motorized with a prescribed velocity. For a desired spooling velocity \dot{L}_t of the tether, the angular velocity of the winch is simply

$$\omega_w = \frac{\dot{L}_t}{r_w + r_t} \quad (2.3)$$

In a physical system such as the one presented by Lanzani, the tether would be coiled several times around the winch in a certain number of layers and thus spooling the tether in or out would constantly vary the amount of tether wrapped around the winch. In Vortex Dynamics, the first segment of the tether is wrapped 180 degrees around the winch and fixed, without coiling. If the winch is reeling in, sections (i.e, rigid bodies) are removed from the tether and if the winch is reeling out, sections are added to the tether. The model of the winch in Vortex Dynamics is shown in Fig 2.6. This model assumes the winch to be an *ideal* actuator.

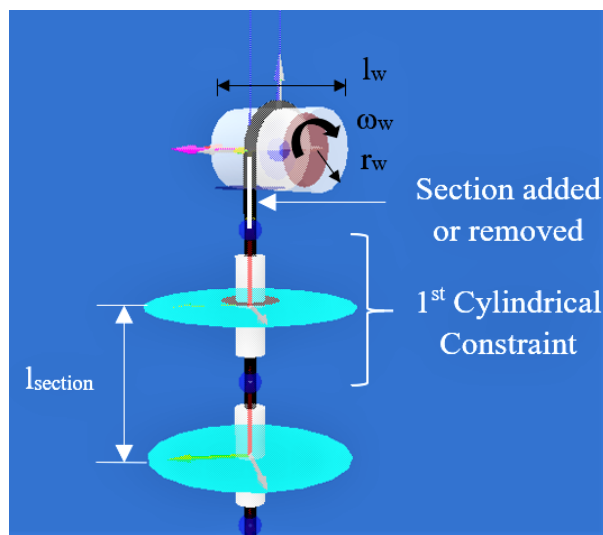


Fig. 2.6 Winch model with tether constraints.

The dynamics equation of the winch is simply:

$$I_w \dot{\omega}_w + C_d \omega_w = \tau_w - T_t(r_w + r_t) \quad (2.4)$$

where I_w is the moment of inertia of the winch, C_d is the motor damping coefficient, T_t is the tension in the tether, and τ_w is the torque exerted by the winch if it is motorized. For the research presented in thesis, motor damping is assumed to be negligible and therefore $C_d = 0$.

2.3 System Assembly

The chaser spacecraft, winch, tether, and net are put together in a single *assembly* in Vortex Dynamics shown in Fig 2.7. The chaser is modelled as a cubic rigid body with side length L_{chaser} and mass m_{chaser} and has zero thrust control. The net is stored at a distance d_{ch} from the bottom of the chaser and in an area $\alpha_{net}^2 L_{net}^2$ where α_{net} is the ratio of initial side length $L_{net,0}$ to nominal side length L_{net} , called the *stowing ratio*. In a physical system the net would be stowed by following a specific folding pattern, meaning that its threads would overlap one another in several layers.

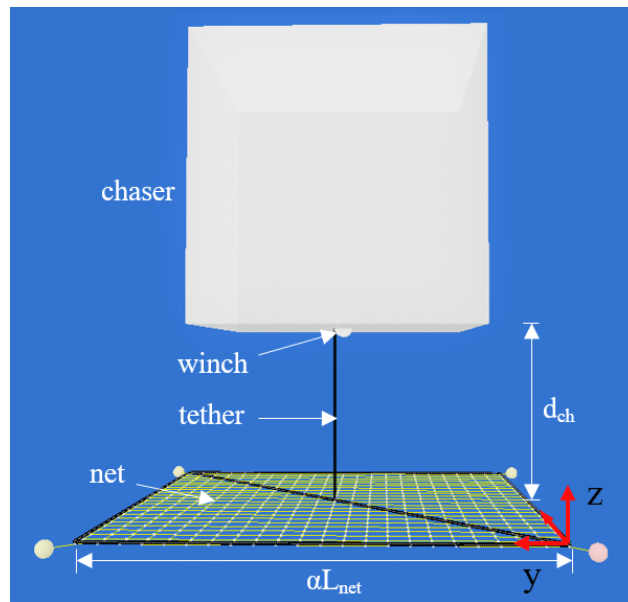


Fig. 2.7 Assembly of the system.

Chapter 3

Simulation and Analysis of Deployment

In this chapter, simulations of the deployment of the net with single tether and double tether-actuated closing mechanisms are performed. For evaluating the performance, several quality indices are drawn from existing research on the deployment of tethered-nets. The effect of tension in the tether is also discussed for both closing mechanism configurations. Having good deployment of the tethered-net system is paramount for successful capture of space debris, and the results from this chapter will aid in determining a nominal capture scenario for Chapter 4.

3.1 Initial Conditions

The net is ejected from the chaser spacecraft by imparting an initial velocity v_{CM} to each of the four corner masses at an angle θ , called the *shooting angle*. The shooting angle is made with the local z-axis of each corner mass. The x and y components of the corner mass' velocity are equal so that deployment is symmetric and the direction of net ejection is parallel to the z-axis of the inertial reference frame. Tensioning of the net threads, starting with the corner threads, causes the net to deploy downwards and the net area to expand. During deployment, the tether is free to spool out as it is tensioned by the net.

3.2 Deployment Quality Indices

It is first necessary to define quality indices which will be used for evaluating the deployment of the net, with the goal of achieving a deployment scenario in which capture of a target debris is possible.

The quality indices are drawn from [8] and [13], and are described as follows:

- *Maximum deployment area* achieved by the net over time. This is represented as the ratio of current net area to the maximum possible net area A_{net}/L_{net}^2 . The area calculated is the area of the polygon projected onto the xy -plane by the *mouth* of the net. The mouth of the net is the set of nodes forming the perimeter of the net proper.
- *Distance travelled* by the center of mass of the net proper with respect to its initial position. A comparison of maximum deployment area to distance travelled is necessary as it suggests how far from the target debris the chaser spacecraft must be to ensure that the net opens sufficiently for capture.
- *Effective period* - how long the maximum deployment area remains above a certain threshold. The deployment area is compared to the net's designed maximum area, L_{net}^2 . A value of $A_{net}/L_{net}^2 \geq 0.8$ is the threshold used in [8] and [13].

Quantitative properties of the tether must also be defined, as they are necessary for assessing the effect of the tether-actuated closing mechanism on the deployment of the net, and for developing the control strategies presented in Chapter 4.

- *Tether length*, L_t , and *spooling velocity*, \dot{L}_t , with a free winch. This will be important when motorized control of the winch is employed for capture.

- *Maximum tension, T_{max}* , throughout the length of the tether, as well as tension in various constraints along the perimeter segments of the tether, particularly at the corners. Due to the complex dynamics of the tethered-net system, it is expected that the tension will vary with time and with position along the tether for the duration of deployment. While measuring tension at several sections along the perimeter segments of the tether is not realistic, for the purpose of evaluating deployment it is necessary for assessing the effect of tension on the net's maximum deployment area.

3.3 Simulation Parameters

The effects of key parameters on the net deployment were investigated by Botta in [8]. These parameters included the mass ratio M_{CM}/M_{total} , the corner mass ejection velocity, the shooting angle, and the net proper ejection velocity. In [8], results were presented for the deployment of a free net without a tether around the perimeter nor attached to the center, and the following conclusions were made:

- M_{CM}/M_{total} has a significant effect on the maximum deployment area and the effective period. It was determined that the maximum deployment area increases as M_{CM}/M_{total} increases from 0.4 to 0.9, however the effective period decreases quickly when $M_{CM}/M_{total} > 0.7$.
- The maximum deployment area is relatively the same for shooting angles between 30° and 45° , and starts to decrease for angles greater than 45° .
- The magnitude of v_{CM} has little effect on the maximum deployment area, but effective period decreases as v_{CM} is increased.

- Ejecting the net proper at an initial velocity v_{net} along the z-axis does not improve the quality of deployment.

These results were used as a guideline for determining a set of parameters for simulating the deployment of the net with the tether-actuated closing mechanism. Geometric and inertial properties of the system are presented in Table 3.1. The corner masses were calculated using a mass ratio $M_{CM}/M_{total} = 0.7$ where the total mass is now $M_{total} = M_{net} + M_{CM} + M_{t,perim}$, in which $M_{t,perim} = \rho_t \pi r_t^2 L_{t,perim}$. The material used for the net and tether is Technora, a high strength polyaramid fiber, and the material used for the corner masses is aluminum. The stiffness and damping properties of Technora were estimated from tests in [14].

Table 3.1 System properties

Net					
L_{net} (m)	l_{mesh} (m)	r_{net} (m)	E_{net} (GPa)	ρ_{net} (kg/m ³)	M_{net} (kg)
22.0	1.0	0.0005	70	1390	1.12
Chaser			Tether		
L_{ch} (m)	m_{ch} (kg)	l_{sec} (m)	r_t (m)	E_t (GPa)	ρ_t (kg/m ³)
1.5	1600	0.1	0.002	70	1390
Corner Masses			Winch		
m_{CM} (kg)	l_{CT} (m)	r_{CT} (m)	m_w (kg)	r_w (m)	l_w (m)
0.75	1.414	0.0007	0.1	0.05	0.14

3.4 Deployment with a Free Tether

The deployment of the net with the two closing mechanism configurations are compared to each other and to a nominal case in which there is a single tether only attached at the central node of the net. The simulations are run for 20 seconds with a time-step of 0.001 s, and data is saved every 0.05

s. The initial conditions are the same for each of the 3 cases and are shown in Table 3.2.

Table 3.2 Initial conditions

v_{CM} (m/s)	θ ($^\circ$)	v_{net} (m/s)	α_{net}	d_{ch} (m)	ω_w (rad/s)
2.5	40	0.0	0.1	2.0	<i>free</i>

It was observed immediately that the deployment of the net with the single tether-actuated closing mechanism was much poorer than with the double tether-actuated closing mechanism. Fig 3.1 shows snapshots of the simulations for the three cases at $t = 10$ s and $t = 15$ s. The corresponding plots of tether spooling velocity, deployment area versus distance travelled, maximum tension in the tether, and tether length are shown in Fig 3.2. The single tether-actuated closing mechanism prevents the net area from expanding beyond $A_{net}/L_{net}^2 = 0.2$ and the net even begins to fold in on itself near the end of the simulation. In addition, the main segment of the tether becomes very slack and spools out at an increasing rate. Lastly, the maximum tension in the tether is significantly higher for the single tether-actuated closing mechanism throughout the simulation. Comparing the double tether-actuated closing mechanism to the case with the tether attached only at the center of the net, the area increases at a slower rate but still reaches the threshold of $A_{net}/L_{net}^2 = 0.8$. The main tether segments remain relatively taut and spool out at a reasonable rate. Note that the measurements shown are for just one of the tethers in the double tether configuration. For both closing mechanism configurations, the onset of tension begins much earlier than the case with the tether attached only at the center of the net. This is because of the segments of tether along the diagonal and around the perimeter of the net. The tether starts to spool out as soon as the corner threads are in tension, whereas for the nominal case the tether only spools out once all of the net

threads have been tensioned. For all cases the distance travelled was similar, ranging from 27 to 32 m.

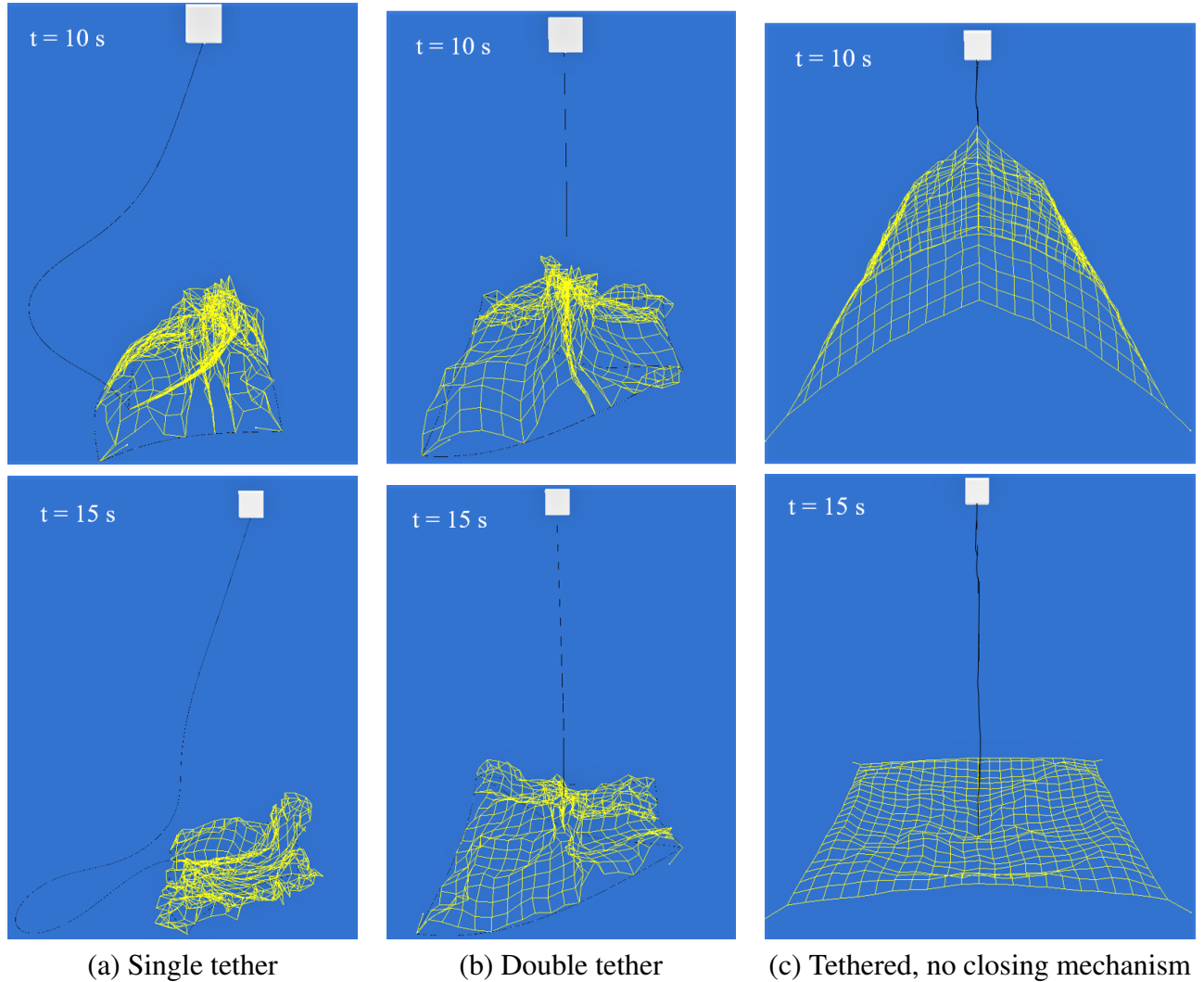


Fig. 3.1 Snapshots of the preliminary deployment test at $t = 10$ s and $t = 15$ s.

The quality of deployment with a single tether-actuated closing mechanism and double tether-actuated closing mechanism is significantly affected by tension in the perimeter segments of the tether. Tension was measured in 5 constraints along the first half of perimeter segments of the tether indicated in Fig 3.3 (a), and the measurements are compared in Fig 3.3 (b). There is a noticeable difference in the magnitude of tension and the frequency of spikes in tension between the two cases.

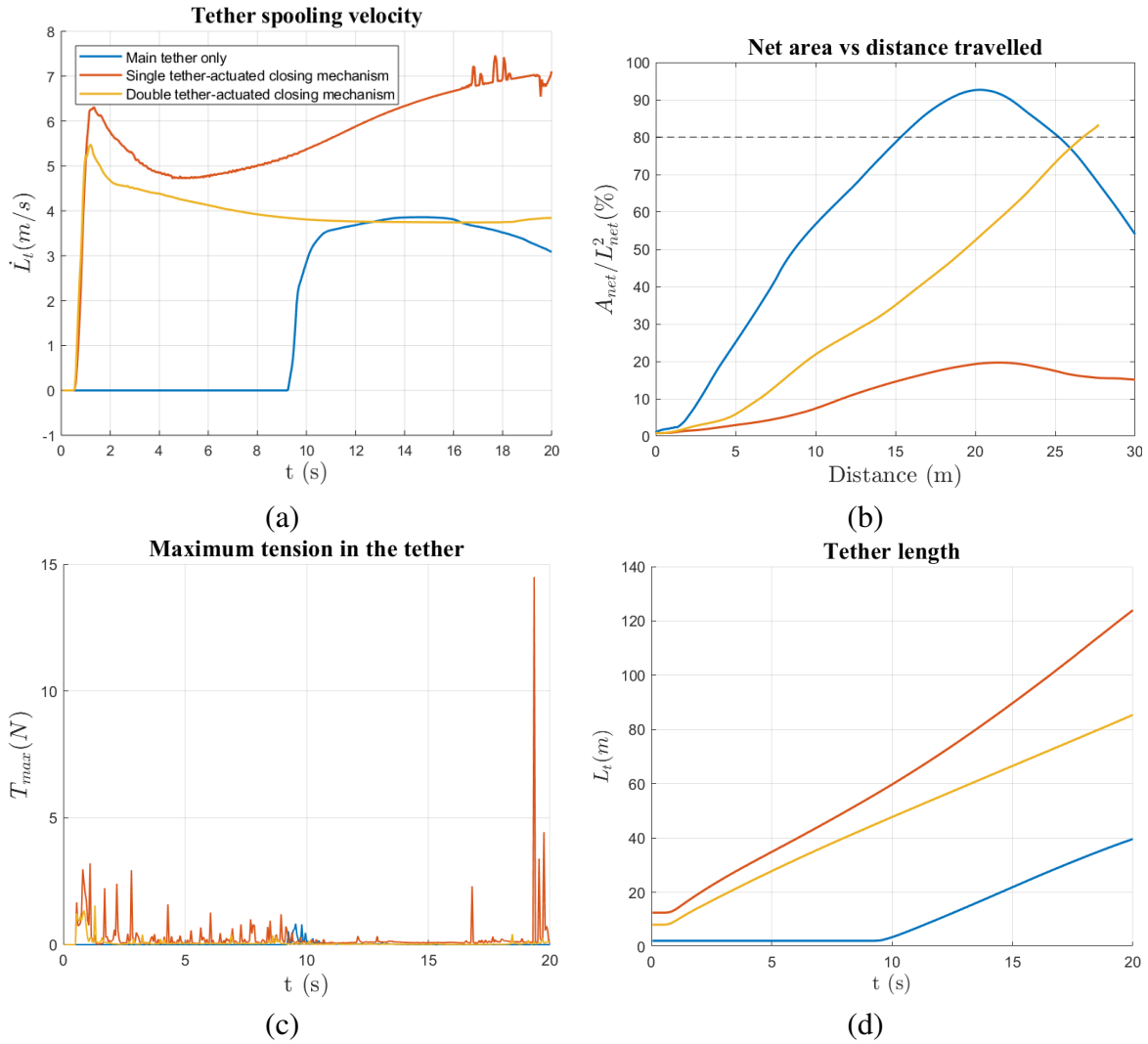
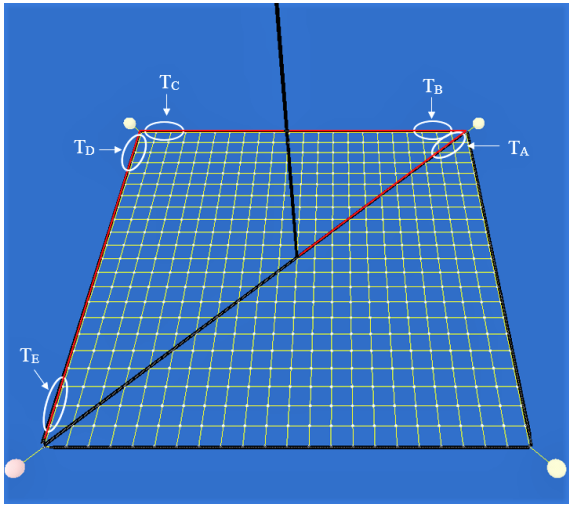
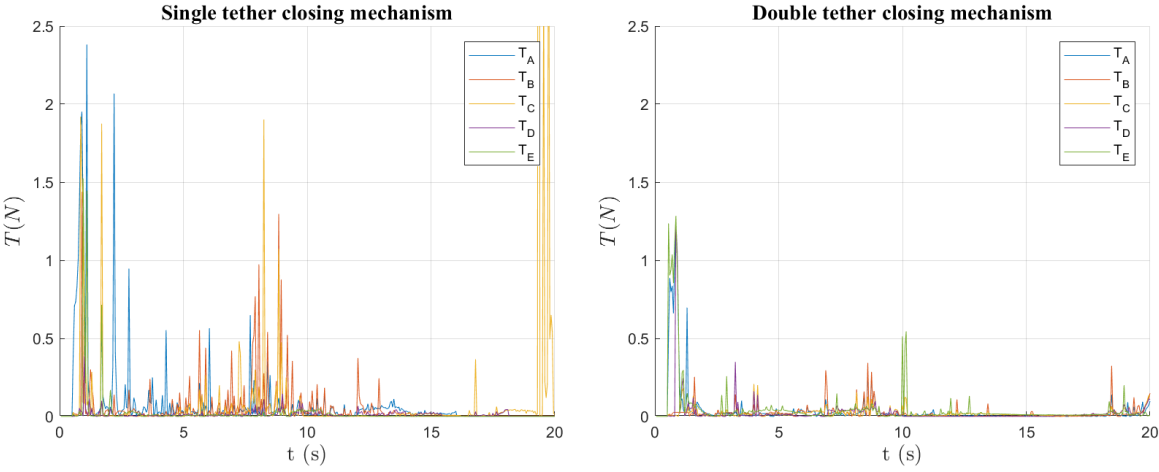


Fig. 3.2 Net and tether deployment characteristics.

The single tether case shows tension at points B and C consistently exceeding a magnitude of 0.5 N, and even 1 N at some instances, whereas for the double tether case the tension at these points rarely exceeds 0.2 N. The increase in tension in the single tether between $t = 8$ s and $t = 10$ s also explains the increasing spooling velocity in Fig 3.2 (a). Overall, the results indicate that the tension in the single tether-actuated closing mechanism hinders the deployment of the net quite significantly, and therefore the single tether configuration is deemed a non-feasible option. The remainder of this thesis focuses on the double tether-actuated closing mechanism.



(a)



(b)

Fig. 3.3 Tension in the perimeter segments of the tether.

Chapter 4

Control of the Tether-Actuated Closing Mechanism

In Chapter 3, simulations of the deployment of the net with single and double tether closing mechanisms were performed. It was observed that due to tension in the perimeter segments of the tether, the single tether-actuated mechanism prevents the net from opening up to an area sufficient for capture, and as a result this configuration is deemed non-feasible. The double tether-actuated closing mechanism showed promising results, and will be used for the simulations of capture presented in this chapter. First, a brief review of the capture dynamics in Vortex is discussed. In the following section, key qualitative criteria for debris capture and containment are presented. The remainder of the chapter focuses on the design and simulation of open loop and closed loop control strategies for capture and containment of a target debris with the tether-actuated closing mechanism.

4.1 Capture Dynamics

Vortex Dynamics uses built-in collision detection algorithms for accurately modelling collision events between multiple rigid bodies. Each body in the simulation is assigned a collision geometry, and the selection of these geometries is based on a balance between computational efficiency

and accurate collision modelling. For the research presented in this thesis, only simple collision geometries are chosen. For example, the net has spherical collision geometry at its nodes and at the corner masses, and the tether has a capsule like collision geometry representing each tether section. The target debris presented in Section 4.1.1 consists of a combination of multiple cylindrical geometries. Each collision geometry is assigned a material with collision related properties such as coefficient of friction and contact stiffness. Contact forces are modelled using the Kelvin-Voigt model and friction forces are modelled with an approximation to the Coulomb friction model: the scaled box friction model [8]. The material properties of each body are stored in a look up table and are called upon to calculate the dynamic response between colliding bodies when a contact is detected.

4.1.1 Target Debris

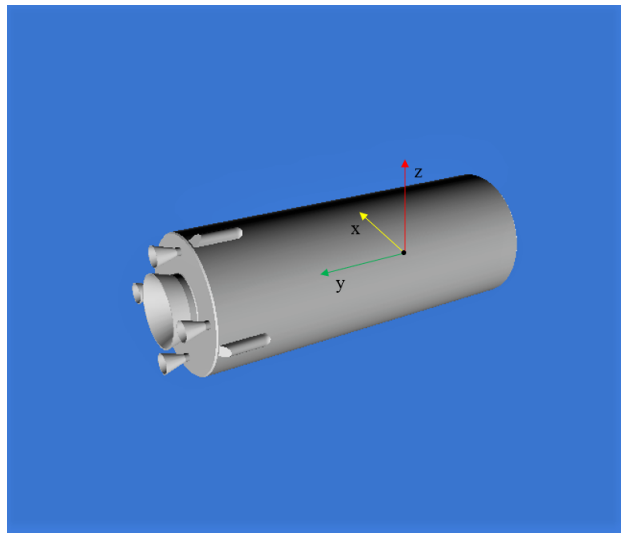


Fig. 4.1 Model of a Zenit 2 upper stage in Vortex Dynamics.

The target debris used for simulations of capture is a Zenit-2 rocket upper stage, shown in Fig 4.1. It has a mass of 9000 kg, a length of 11 m and a diameter of 3.9 m. The inertia matrix was estimated by approximating the debris as a thick-walled cylindrical tube with open ends [8]. For the reference

frame shown in Fig 4.1, the inertia tensor of the Zenit-2 upper stage is:

$$\mathbf{I}_G = \begin{bmatrix} 94880 & 0 & 0 \\ 0 & 46295.5 & 0 \\ 0 & 0 & 94880 \end{bmatrix} \text{ kg m}^2 \quad (4.1)$$

4.1.2 Criteria for Capture and Containment of Debris

Due to the complex dynamics of the system, overall *qualitative* criteria are drawn from [8] and used for evaluating capture of a target debris with the tether-actuated closing mechanism:

- *Closure* of the net around the target debris. If the perimeter segments of the tether remain underneath the target debris for the entire duration of the closure phase, then closure is successful.
- *Slip-off*, characterized by an increase in net area after attempted closure of the net. This will occur if any of the perimeter segments of the closing mechanism do not remain underneath the target.
- *Containment* of the debris once closure of the net is achieved. This is crucial for the post-capture phase of the ADR mission, as the chaser spacecraft would then need to tug the target to a disposal orbit.

4.1.3 Nominal Capture Scenario

It is assumed that the position of the target is known, and that after rendezvous with the debris and prior to initiating deployment of the net the distance between the target and chaser spacecraft

remains constant and the target has zero angular velocity. The target is oriented such that the axis of its main cylinder is parallel to the xy -plane and intersects the net's deployment axis, as shown in Fig 4.2. The initial conditions used for all simulations in this chapter are shown in Table 4.1. In Chapter 3, a threshold of $A_{net}/L_{net}^2 = 0.8$ was used for evaluating the deployment of the net with the tether-actuated closing mechanism. However, it was observed that the net begins to fold up on itself once the area of the net reaches 70% of its maximum possible area, and the diagonal segments of the tether-actuated closing mechanism surpass the center of mass of the net proper. Therefore, for simulating capture of the chosen target debris the initial distance d_{target} was set to 22 m, such that the net area is roughly 60% of its maximum possible area when the first contact with the surface of the target debris occurs. This is reasonable due to the size of the net and the size of the target debris. The position of the center of mass of the target is offset slightly from the net's deployment axis such that envelopment by the net is symmetric. With respect to the reference frame shown in Fig 2.7, the position of the target's center of mass is $\mathbf{r}_G = [1.1 \quad -0.65 \quad -23.95]$ m.

Table 4.1 Initial conditions for simulation of capture.

v_{CM} (m/s)	θ ($^\circ$)	v_{net} (m/s)	α_{net}	d_{ch} (m)	ω_w (rad/s)	d_{target} (m)
2.5	40	0.0	0.1	2.0	<i>variable</i>	22

4.2 Open Loop Control Strategy

An open loop control strategy is employed as a preliminary test of debris capture with the tether-actuated closing mechanism. Results from this section will be used as a starting point for the design of the closed loop control law in Section 4.3.

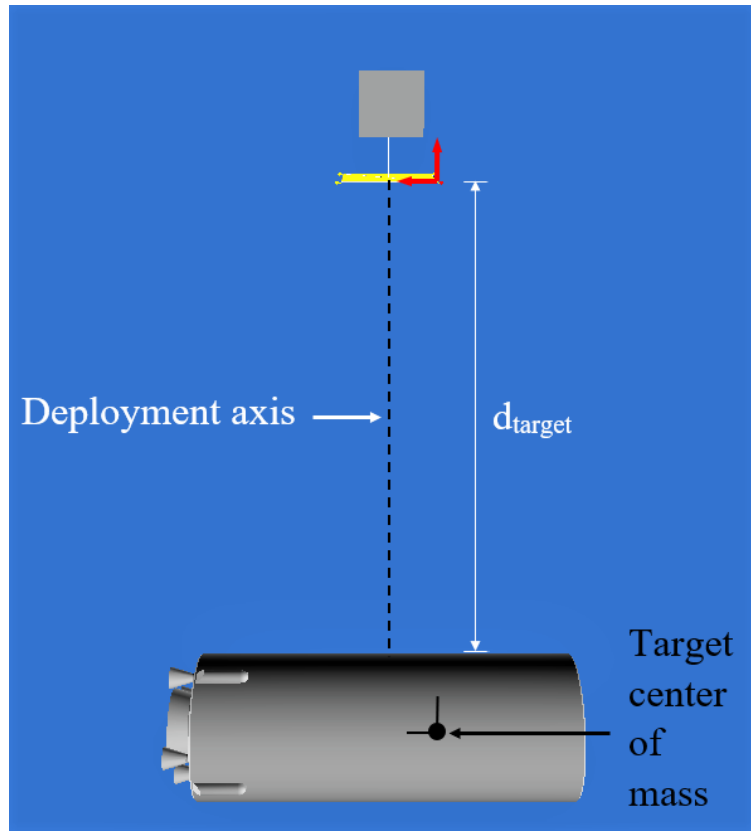


Fig. 4.2 Nominal capture scenario.

4.2.1 Measurable Parameters

It is important to consider which parameters of the system could realistically be measured, or at least estimated. It would not be possible to measure the mouth area of the net because the positions of each node of the net are unknown and therefore the most important measurements will be those of the tether and of the winch. The control input for both the open loop and closed loop control strategies discussed in this chapter is the winch angular velocity, ω_w . It is assumed that the appropriate sensors are placed at, or near, the winch to measure the length of each tether L_t , spooling velocity \dot{L}_t , and the torque on the winch τ_w . Furthermore, it is possible to measure at any point in time the relative position, velocity, angular velocity, and acceleration of the chaser spacecraft.

4.2.2 Angular Velocity Control of the Winch

The general idea of the open loop control strategy is described as follows: First spool the tether out in a controlled way to allow the net to begin enveloping the target; next, spool the tether in to a desired length to close the perimeter of the net around the target. For a desired spooling rate \dot{L}_t of the tether, the angular velocity ω_w input to the winch is simply:

$$\omega_w = \frac{\dot{L}_t}{r_w + r_t} \quad (4.2)$$

The closing mechanism is actuated by prescribing a piecewise angular velocity function to the winch and consists of three phases: *free deployment*, *controlled spooling-out*, and *closure*. Practical limits on tether spooling velocity for tethered-net systems have been investigated by Lanzani for the conceptual design of a reel mechanism such as the one presented in Chapter 2. It was reported that during controlled deployment, the tether spooling velocity should not exceed 5 m/s outward, and during retrieval, the tether spooling velocity should not exceed 2 m/s inward [12]. These limits are used as a guideline for the open loop control of the tether spooling velocity discussed in this section.

The timing of the controlled spooling-out phase and the closure phase of the open loop control strategy is vital to the tethered-net's ability to capture and contain the debris. The initial collision with the target debris is the main event that determines the timing of the open loop control. Once the collision is detected, controlled spooling-out of the tether will begin. An initial simulation was performed to determine how the initial collision between the net and target effects the tether winching velocity and maximum tension in the tether, because it is likely that the impulse will cause a jump in both of these parameters. Fig 4.3 shows the results of this test. As expected, there is a sudden drop in tether spool-

ing velocity and a spike in maximum tension in both of the tethers at $t = 16.3$ seconds, indicating that the net and tether have impacted the debris. However, using the initial impact as the time to initiate controlled spooling-out of the tether could be dangerous in a real ADR scenario because of the unpredictable dynamics of the situation. In addition, the maximum tension in the tether cannot realistically be measured. Therefore, controlled spooling-out of the tether-actuated closing mechanism should be initiated before the initial collision with the debris. With the use of visual sensors such as Lidars and cameras, as well as reflective markers placed on the corner masses, it would be possible to estimate the positions of the corner masses as long as they are still visible (i.e., not on the other side of the target debris). The time at which one of the corner masses is within some vertical distance from the plane tangent to surface of the target debris can be used as the time to initiate controlled spooling-out of the tether. It was observed in the same initial simulation with the free tether that one of the corner masses reaches a vertical distance of 21 m from its initial position at $t = 15$ s, corresponding to a distance of 1 m from the plane tangent to the surface of the target debris. Thus, for the control strategies described in this chapter, controlled spooling-out of the tether begins at $t = 15$ s in all cases.

Results from a particular simulation with open loop control are shown in Fig 4.4. Controlled spooling-out of the tether begins at $t = 15$ s, indicated by the dashed vertical black line, with a moderate velocity of $\dot{L}_t = 2.5$ m/s. At $t = 18$ s, the rate is decreased to $\dot{L}_t = 1$ m/s until $t = 24$ s, at which point closure is initiated, shown by the dashed vertical red line. The desired tether spooling velocity during the closure phase is shown by the dashed black line, and at $t = 57$ s the winch is locked. The measured \dot{L}_t does not consistently match the desired spooling rate because of elastic elongation and bending throughout the tether over time. At $t = 55$ s the torque on the winch increases sharply indicating that the tethers have reached a critical length and closure of the net around the

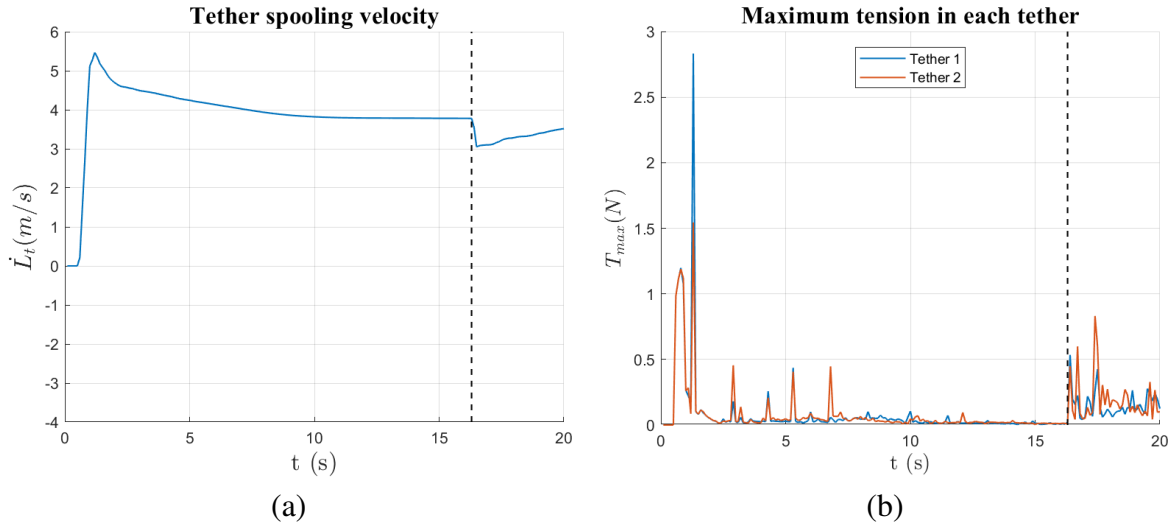


Fig. 4.3 Collision between net and debris with the tether-actuated closing mechanism free to spool out.

debris was successful. However, this sharp increase in winch torque is undesirable as it also suggests that the tether has started to pull on the target, which causes a dangerous reaction on the chaser spacecraft. This presents the need for tension control of the tether-actuated closing mechanism.

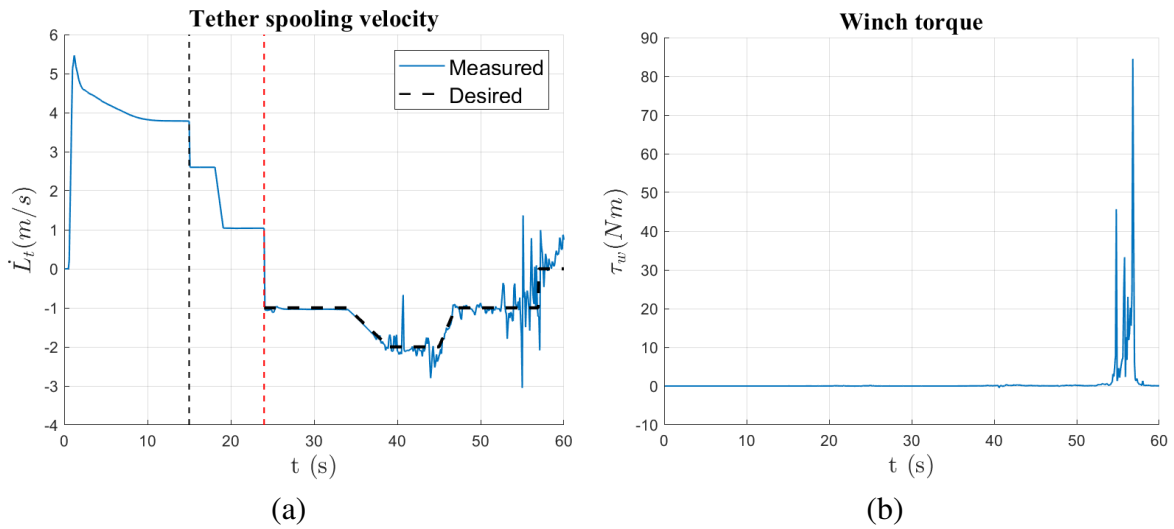


Fig. 4.4 Open loop angular velocity control of the winch.

4.3 Closed Loop Control Strategy

4.3.1 PD Tension Control

Due to limitations in the Vortex Dynamics framework at the time of writing, the tension in this first constraint could not be measured directly. Therefore, the tension in the *first constraint* nearest the winch of one of the tethers is estimated with:

$$T = \frac{\tau_w}{2(r_w + r_t)} \quad (4.3)$$

The PD tension control law is given by:

$$\omega_w = K_p(T - T_{ref}) + K_d \frac{\Delta T}{\Delta t} \quad (4.4)$$

To clarify, the tension T is calculated at every time step using Equation 4.3. In equation 4.4, ΔT is the difference between the tension calculated at the current time step and the tension calculated at the previous time step. To reduce noise in the measurements the PD control law is called every 0.1 s and thus $\Delta t = 0.1$ s in Equation 4.4, whereas the simulation time step remains as 0.001 s. The reference tension T_{ref} , proportional gain K_p , and derivative gain K_d are shown in Table 4.2.

Table 4.2 Reference tension and control gains

T_{ref} (N)	K_p ($\frac{rad/s}{N}$)	K_d ($\frac{rad}{N}$)
20.0	-2.0	0.02

The proportional gain was chosen such that when the estimated tension is near zero, the angular velocity of the winch is approximately 40 rad/s corresponding to a spooling-in rate of 2 m/s. The

derivative gain was tuned through trial and error. Results for a 60-second simulation with these settings are shown in Fig 4.5. As before, controlled spooling-out of the tether begins at $t = 15$ s. At $t = 24$ s the winch is prescribed a constant angular velocity $\omega_w = 20$ rad/s for 10 seconds. The PD tension control law takes over at $t = 34$ s for the remainder of the simulation. A sharp increase in winch torque occurs at $t = 52.3$ s, at which point the tethers have been spooled-in to a length of 36 m, and large oscillations in winch angular velocity and winch torque are observed shortly after this instance. Furthermore, a significant change in the chaser spacecraft's vertical position was observed, indicating that the tethers started to pull the chaser toward the target debris. Although capture of the target debris was successful, these results suggest that control of the tether-actuated closing mechanism can be improved further with gain scheduling based on tether length and change in chaser position. A longer simulation must also be performed to determine if the target debris is contained after closure of the net.

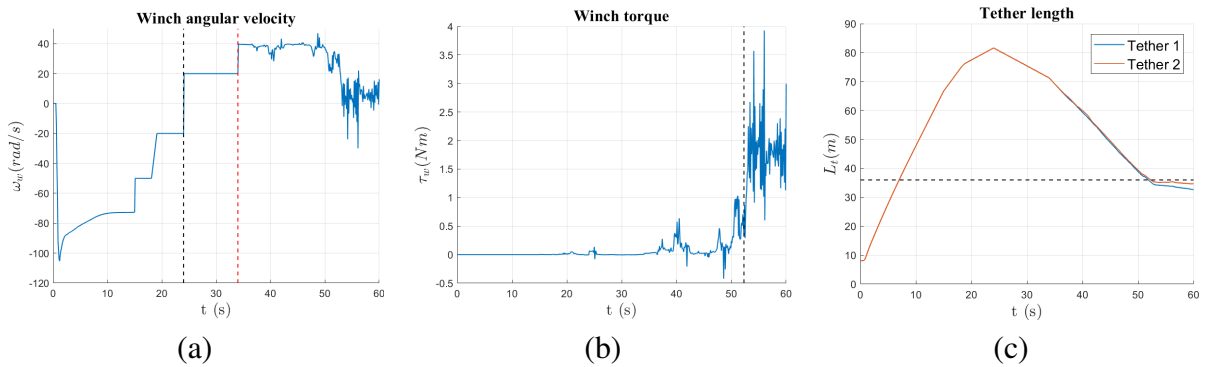


Fig. 4.5 PD tension control of the tether-actuated closing mechanism.

4.3.2 Gain Scheduling

The gain scheduling is employed as follows:

- First, if $\Delta z_{ch} \leq -0.25$ m, the proportional gain is reduced by half and the derivative gain remains the same: $K_p = -1.0$ rad/Ns and $K_d = 0.02$ rad/N.

- Then, if $L_t < 36$ m, the proportional gain is reduced again by half and the derivative gain is also reduced by half; $K_p = -0.5$ rad/Ns and $K_d = 0.01$ rad/N.
- Finally, if $L_t < 33$ m, the proportional and derivative gains remain the same as above but the reference tension is reduced to $T_{ref} = 5$ N.

The choices of the gain scheduling parameters are somewhat arbitrary, and there is a margin to improve the gain scheduling scheme.

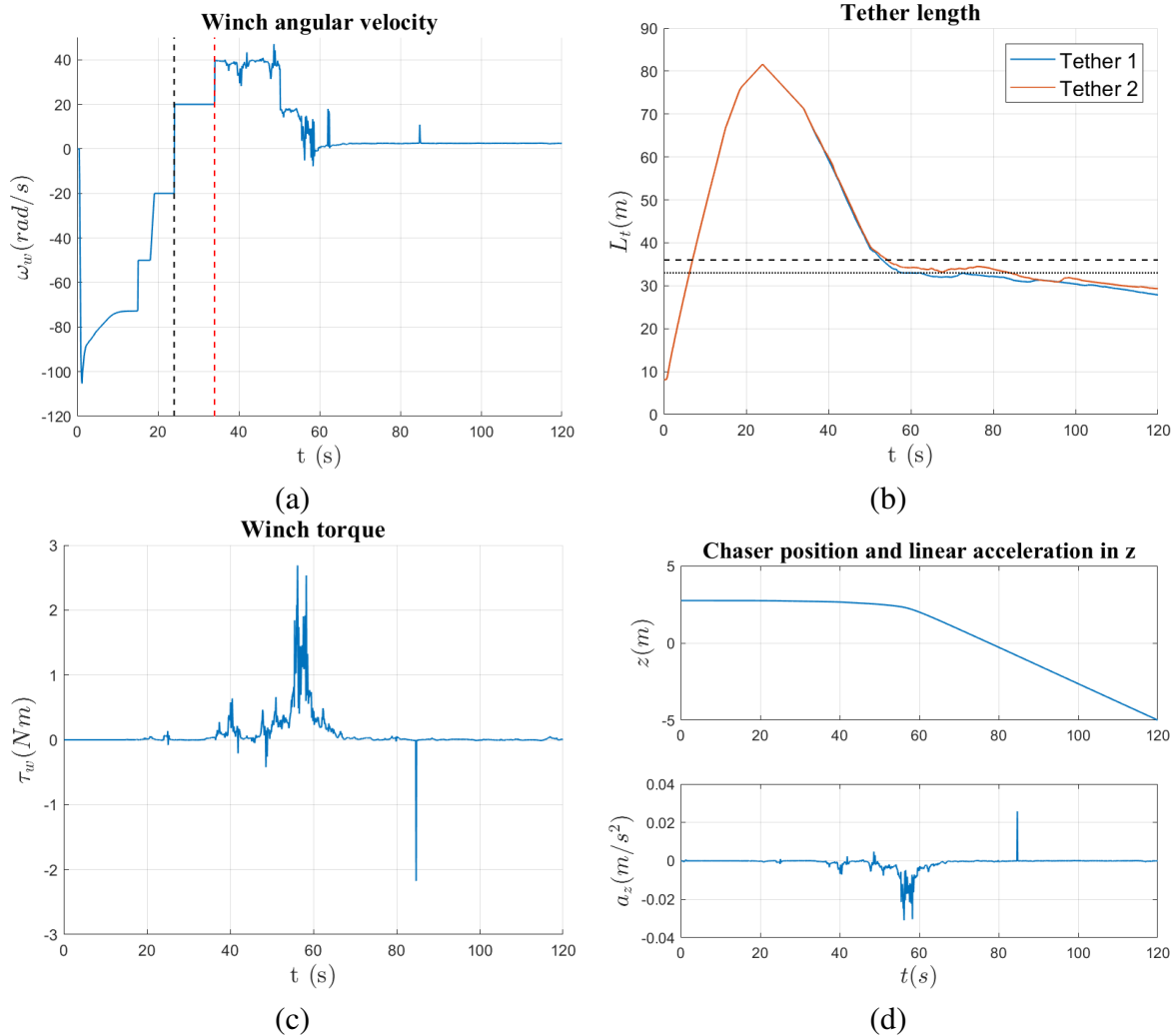


Fig. 4.6 Results from simulation of debris capture with PD tension control with gain scheduling

The simulation time was extended to 120 s and results are shown in Fig 4.6. At $t = 53.1$ s, $L_t = 36$ m, torque on the winch increases, and the chaser experiences significant linear acceleration toward the target in the negative z -direction. By $t = 58$ s, $L_t = 33$ m and T_{ref} is now 5 N. The torque on the winch decreases and remains negligible despite a brief spike at $t = 82.3$ s. The dashed line and dotted line in Fig 4.6 (b) mark $L_t = 36$ m and $L_t = 33$ m, respectively. The angular velocity of the winch remains relatively constant around 2.5 rad/s once T_{ref} has been reduced, but the chaser moves at a constant rate toward the target for the remainder of the simulation. This is attributed to the peak in winch torque of 2.7 Nm measured at $t = 56.2$ s. Using Equation 4.3 and accounting for the second tether, the estimated total tether tension at this instance is 51.9 N. By Newton's second law, the chaser spacecraft experiences a linear acceleration of 0.032 m/s² toward the target debris at $t = 56.2$ s, as shown in Fig 4.6 (d). Fig 4.7 shows snapshots of the simulation at $t = 50$ s, $t = 80$ s, and $t = 120$ s, highlighting the change in chaser position. The total change in the chaser's vertical position z_{ch} is -7.74 m. This is undesirable as it increases the likelihood of a collision with the target debris, and it causes the tether to go slack, thus losing control authority of the tethered-net system.

One solution to this problem would be to activate thruster control on the chaser spacecraft for stabilization of the entire system post-capture. However, this is beyond the scope of this work and a simpler solution is employed. Vortex Dynamics allows components of the system to be fixed in a desired position at the discretion of the user. Thus, to emulate thruster control on the chaser spacecraft, the chaser part can be fixed in space as if the spacecraft is *station-keeping*. This is a term used in spacecraft dynamics meaning that thruster burns are used to keep the spacecraft in a particular assigned orbit. A final simulation was performed using the same gain scheduling as listed above. This time, the chaser spacecraft was set to be fixed once its vertical position z_{ch} had decreased

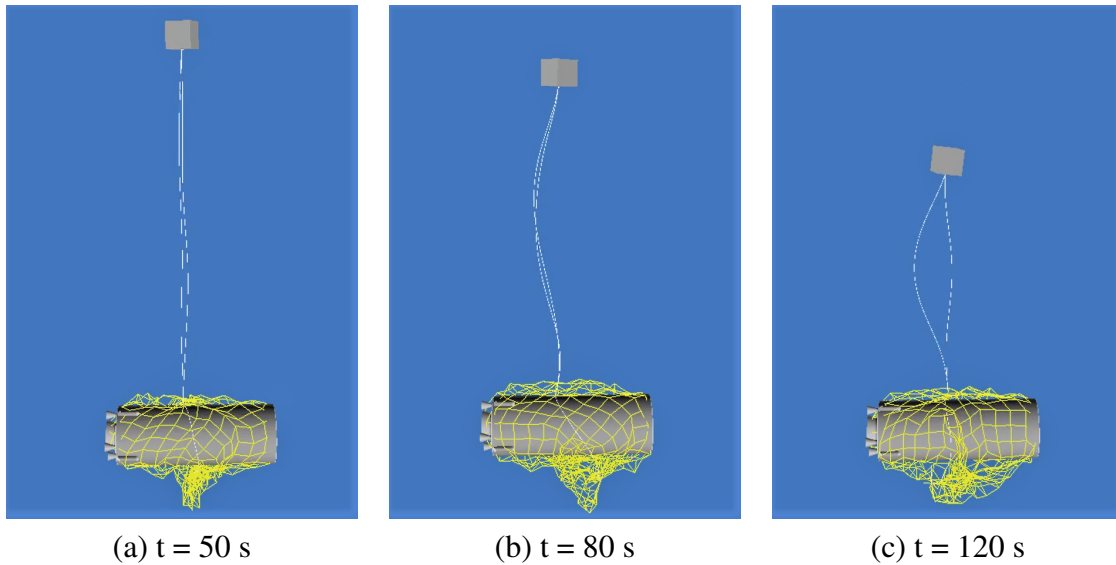


Fig. 4.7 Snap shots from simulation of debris capture with PD tension control and gain scheduling.

by 0.25 m. This is the same moment at which the proportional gain is first reduced to $K_p = -1.0$ rad/Ns. The results from this simulation are shown Fig 4.8. The chaser spacecraft's position is fixed at $t = 50.2$ s, indicated by the vertical dashed line in Fig 4.8 (d), and at the same instance there is a sharp increase in winch torque. However once the tether length reaches 36 m and the gains are reduced, both the winch torque and rate of change of tether length decrease significantly. Once the reference tension is reduced to $T_{ref} = 5$ N, the tether length is kept relatively constant at $L_t = 33$ m. The spooling velocity of the tether remained within the practical limits suggested by Lanzani.

4.4 Discussion of Results

Throughout the development of the open loop and closed loop control strategies presented in this chapter, several challenges were encountered. The results presented in this chapter were obtained through an extensive trial and error process. In the first simulations using open loop control, it was realized that the net's ability to capture the debris depends heavily on the timing of the controlled spooling-out and closure phases, as well as on the spooling velocity during in both phases. During

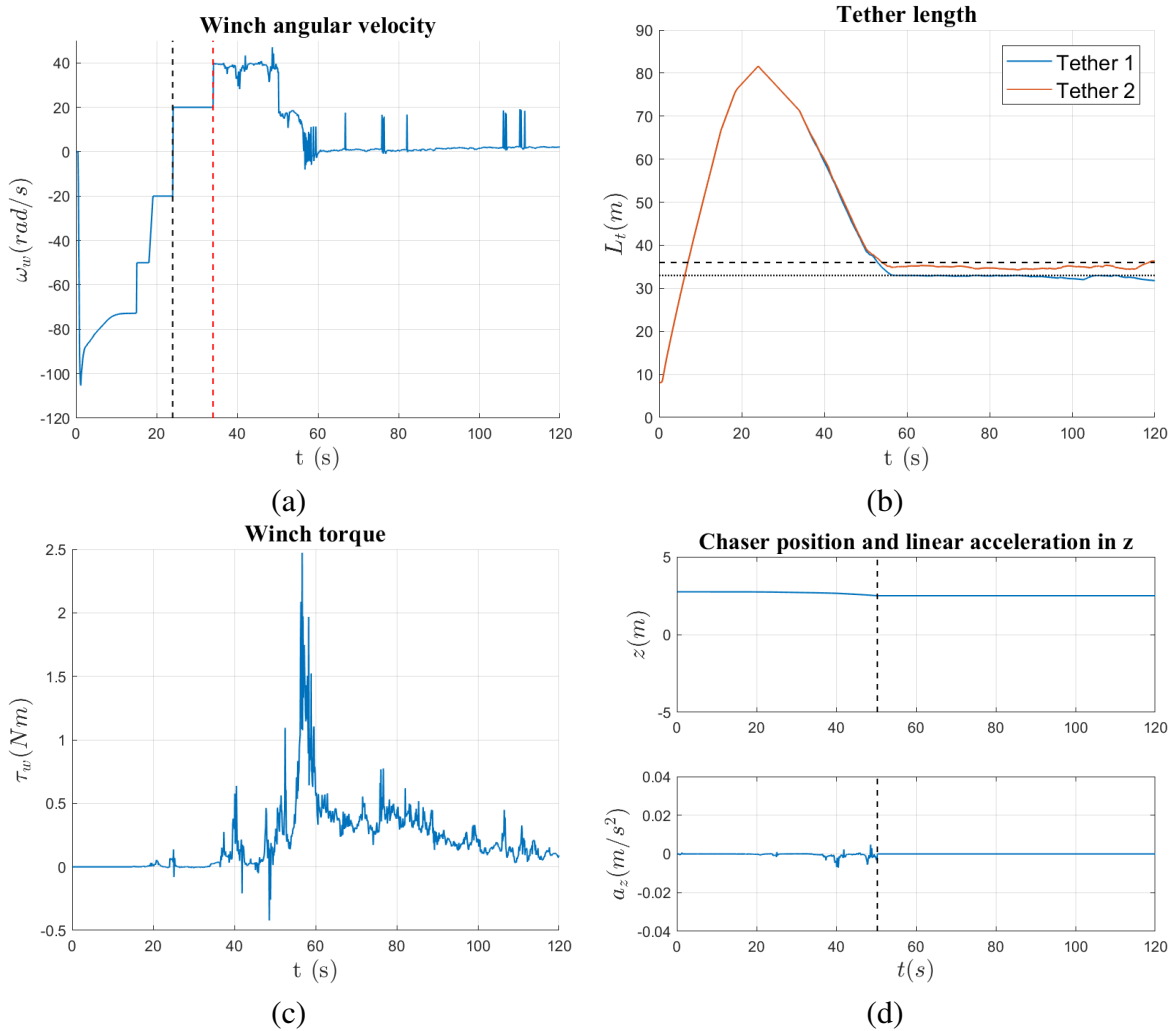


Fig. 4.8 PD tension control with gain scheduling and emulated thruster control of the chaser spacecraft.

controlled spooling-out of the tether, if the spooling velocity is too high the net fails to envelop the target debris, and eventually slips off the debris during closure. Slip-off was also observed if the magnitude of the spooling velocity during closure exceeded 3 m/s. PD tension control with gain scheduling and emulated thrust control on the chaser spacecraft resulted in successful capture and containment of the target debris. The tether spooling velocity remained within the practical limits suggested by Lanzani, and the tether length remained relatively constant once the reference tension was reduced. However, additional undesirable behaviour in the tether was observed. Tension in the

tether during containment of the debris caused transverse vibrations along the main tether segment between the chaser and the debris, and these vibrations could not be eliminated with the PD control law. For stabilization of the system during containment of the debris, a more sophisticated control law is needed, coupled with proper thruster control of the chaser spacecraft.

Chapter 5

Conclusion

5.1 Main Findings

The research conducted for this thesis focused primarily on the development of a model and a control scheme for a tether-actuated closing mechanism for net-based capture of space debris. Much of the work presented extends from that of Botta, who developed a Vortex Dynamics based simulator for debris capture with tethered-nets. The simulator was used and improved upon for the simulation and control of the tether-actuated closing mechanism.

First, a model of the tethered-net ADR system was implemented in the Vortex Dynamics simulator. A standard lumped parameter model was used to represent the net and the tether was represented with Vortex's flexible cable model. Two configurations for the tether-actuated closing mechanism were then designed. Existing research on the conceptual design of a reel mechanism was discussed and compared to the winch model employed in the simulator. The tethered-net system was then put together in an assembly with a simplified model of a chaser spacecraft.

Deployments of the net with the single tether-actuated closing mechanism and double tether-actuated closing mechanism were compared in simulation to a nominal case in which the tether was attached only to the center of the net. Quality indices for evaluating deployment of the tethered-net were drawn from literature and used in the comparison of results. It was determined that the single-tether configuration was non-feasible, because tension along the perimeter segments of the tether prevented the net from expanding beyond 20% of its maximum achievable area.

Characteristics of the deployment of the net with the double tether-actuated closing mechanism were used to determine a nominal capture scenario. An open loop control strategy based on winch angular velocity control was implemented. It was determined that spooling-in of the tether closes the net around the debris, but tension control is needed for containment of the debris. In light of this result, a PD tension control law with gain scheduling, as well as emulated thruster control on the chaser spacecraft, was applied. This control law demonstrated capture and containment of the target debris while keeping the tension and spooling rate of the tether within realistic limits. Ultimately, thruster control on the chaser spacecraft is needed for stabilization of the system post-capture.

5.2 Suggestions for Future Work

Through the research on the simulation and control of the tether-actuated closing mechanism, much was learnt about its application in an active debris removal scenario. The results show that capture and containment of debris is feasible through PD tension control of the tether, yet some issues still remain open. Some of the issues encountered and suggestions for how to address them are discussed in the this section.

The control scheme for the tether-actuated closing mechanism needs further development. It was demonstrated that the timing of the actuation of the closing mechanism is critical to the system's ability to capture and contain the debris. Therefore, optimization of the control law could be explored. One approach could be to use a genetic algorithm to find the optimal timing of the controlled-spooling out and closure phases. This, as well as further tuning of the gains and gain scheduling parameters could drastically improve the control law for the tether-actuated closing mechanism.

As mentioned in Chapter 4, thruster control on the chaser spacecraft is needed stabilize the system in the post-capture phase. This would increase the number of degrees of freedom through which the system can be controlled, and could eliminate some of the undesired behaviours that were observed, such as vibrations in the main segment of the tether. In addition, control of the chaser spacecraft is need for the de-orbiting phase of the mission.

The model of the winch can also be improved by incorporating additional components such as a level-wind, grip-pulley and brake system. This would bring the model of the winch closer to the reel-mechanism design proposed by Lanzani. Furthermore, the control authority on the tether would improve and would allow for even further development of the control system. Implementing realistic motor limits such as damping, friction and efficiency would make the model more realistic.

References

- [1] D. J. Kessler and B. G. Cour-Palais, “Collision frequency of artificial satellites: The creation of a debris belt,” *Journal of Geophysical Research: Space Physics*, vol. 83, no. A6, pp. 2637–2646, 1978.
- [2] C. Bonnal, J.-M. Ruault, and M.-C. Desjean, “Active debris removal: Recent progress and current trends,” *Acta Astronautica*, vol. 85, pp. 51–60, 2013. [Online]. Available: <http://dx.doi.org/10.1016/j.actaastro.2012.11.009>
- [3] ESA Space Debris Office, “ESA’s Annual Space Environment Report,” European Space Agency, Tech. Rep., 2018. [Online]. Available: <https://www.esa.int/Our{ }Activities/Operations/Latest{ }report{ }on{ }space{ }junk>
- [4] J.-C. Liou, N. L. Johnson, and N. M. Hill, “Controlling the growth of future LEO debris populations with active debris removal,” *Acta Astronautica*, vol. 66, no. 5-6, pp. 648–653, 2010. [Online]. Available: <http://dx.doi.org/10.1016/j.actaastro.2009.08.005>
- [5] C. Wiedemann, S. Flegel, M. Möckel, J. Gelhaus, V. Braun, C. Kebschull, J. Kreisel, M. Metz, and P. Vörsmann, “Cost estimation of active debris removal,” in *63rd International Astronautical Congress*, 2012.
- [6] M. Shan, J. Guo, and E. Gill, “Review and comparison of active space debris capturing and removal methods,” *Progress in Aerospace Sciences*, vol. 80, pp. 18–32, 2016. [Online]. Available: <http://www.sciencedirect.com/science/article/pii/S0376042115300221>
- [7] Clean Space, “e.Deorbit Implementation Plan,” European Space Agency, Tech. Rep., 2015. [Online]. Available: <http://blogs.esa.int/cleanspace/2016/02/04/the-e-deorbit-workplan/>
- [8] E. Botta, “Deployment and capture dynamics of tether-nets for active space debris removal,” Ph.D. dissertation, McGill University, 2017.
- [9] I. Sharf, B. Thomsen, E. M. Botta, and A. K. Misra, “Experiments and simulation of a net closing mechanism for tether-net capture of space debris,” *Acta Astronautica*, vol. 139, pp. 332–343, 2017. [Online]. Available: <http://www.sciencedirect.com/science/article/pii/S0094576517303089>
- [10] L. Johnson, E. Lorenzini, B. Gilchrist, N. Stone, and K. Wright, “Propulsive small expendable deployer system (proseps) experiment: Mission overview and status bt,” ser. 39th AIAA/ASME/SAE/ASEE Joint Propulsion Conference and Exhibit. NASA Marshall Space Flight Center: American Institute of Aeronautics and Astronautics Inc., 2003.
- [11] M. Kruijff, E. J. Van Der Heide, W. J. Ockels, and E. Gill, “First mission results of the yes2 tethered spacemail experiment bt,” ser. AIAA/AAS Astrodynamics Specialist Conference and

Exhibit. Delft University of Technology: American Institute of Aeronautics and Astronautics Inc., 2008.

- [12] M. Lanzani, “Reel mechanism design for active debris removal,” Master’s thesis, Politecnico di Milano, 2014.
- [13] M. Shan, J. Guo, and E. Gill, “Deployment dynamics of tethered-net for space debris removal,” *Acta Astronautica*, vol. 132, pp. 293–302, 2017. [Online]. Available: <http://www.sciencedirect.com/science/article/pii/S0094576516309961>
- [14] S. Salvi, “Flexible devices for active space debris removal: the net simulation tool,” Master’s thesis, Politecnico di Milano, 2014.